Ultrabosonic behavior in photoexcited one-dimensional Mott insulators in the region of weak intersite Coulomb interaction

K. Iwano ⬤

Graduate University for Advanced Studies, Institute of Materials Structure Science, High Energy Accelerator Research Organization (KEK),
1-1 Oho, Tsukuba 305-0801, Japan

T. Yamaguchi ⬤

Institute of Materials Structure Science, High Energy Accelerator Research Organization (KEK), 1-1 Oho, Tsukuba 305-0801, Japan

H. Okamoto ⬤

Department of Advanced Materials Science, University of Tokyo, Chiba 277-8561, Japan
and AIST-UTokyo Advanced Operando-Measurement Technology Open Innovation Laboratory, National Institute of Advanced Industrial
Science and Technology (AIST), Chiba 277-8568, Japan

This paper reports a unique behavior expected for the optical excitations in one-dimensional Mott insulators. When the intersite Coulombic attraction does not work between two elementary charge excitations, i.e., a doublon and a holon, the lowest optical excitations are described as an unbound pair of them, still having finite mutual correlation due to the forbidden double occupancy on the same site. We find that, in such a situation, the pairs obey a particle statistics that exceeds that of ordinary bosons. This feature appears most directly in the enhancement factor of the matrix element for the pair photocreation. We discuss the possible mechanism for this *ultrabosonic* behavior and also demonstrate that this behavior is maintained even if we include a small amount of interiste Coulomibic interaction. Lastly, this enhancement factor almost coincides with that for ordinary bosons when the degree of the intersite interaction exceeds a certain value that switches on the formation of a bound doublon-holon pair.

I. INTRODUCTION

The physics of the optically excited states in one-dimensional (1D) Mott insulators has attracted much attention in recent decades [1,2]. One of the pioneering works is the rigorous proof [3] of spin-charge separation [4–10] in the limit of strong on-site repulsion (U) in the 1D Hubbard model. In this theory, the entire Hilbert space is decoupled into the charge sector and the spin sector, including not only the ground state but also any excited state. Subsequent to this work, the low-energy optical excitations have been extensively studied from various viewpoints [11–29].

The lowest optical excitations are described as a pair consisting of a doublon (D) and a holon (H), which are doubly occupied and empty sites of electrons, respectively, in a background of singly occupied sites corresponding to the Mott insulator. One of the striking features of this pair state is the almost degenerate parity-even and parity-odd states of a bound pair, which is completely different from the properties of ordinary excitons in band insulators [13–16]. Recently, further exploration focusing on the spin-charge-separation has been conducted for finite U/T values with T being the nearest-neighbor electron hopping, indicating that this concept holds sufficiently in strong and intermediate U/T regions [30].

However, little is known regarding higher excitations, owing to the complexity of the states, except, for example, a recent study about the biexcitonlike state [31]. We think that higher excitations will become more and more important in the near future. First, the higher excitation beyond one DH pair is important when discussing photoinduced states [32–35], where the higher excitation is the final state of the transition starting from the initial photoinduced state. In other words, the higher excitation is directly related to the *probe* part of the pump-probe experiments. Moreover, intense light excitations inevitably access the higher excitations. The so-called photoinduced phase transitions in such cases are already attracting fields at present and will also continue to in the future.

In this situation, we focus on the multi-DH-pair states and report on their unexpected properties, particularly the characteristic enhancements of the transition matrix element from an n-pair-state to an $(n + 1)$-pair state. To investigate those states, we employ the charge model, which was successfully applied to the (linear) optical conductivity [30]. We now apply it to multi-DH-pair states, since it is shown immediately that the charge model also reproduces the spectra associated with multi-DH-pair states obtained by the Hubbard model. As a result, we found that the ratio of the matrix element to that of $n = 0$ is $\sqrt{3}$ and $\sqrt{6}$ for $n = 1$ and $n = 2$, respectively. Apparently, these numbers exceed those for the ordinary bosons that are $\sqrt{2}$ and $\sqrt{3}$, respectively. This tendency is most outstanding in the absence of the intersite Coulombic repulsion (V),

while it is gradually suppressed with increasing V, toward the case of a bound DH pair showing an ordinary boson behavior.

Particle statistics has been one of the hot issues in the field of condensed matter. As is well known, so-called anyons are defined as particles of neither bosons nor fermions [36,37]. The emerging novel properties have attracted much attention, stimulating their search in various systems. Although our finding about the DH pairs is not of the anyon in the meaning that they do not show any fermionic nature, the present result indicates that they can be interpreted as not ordinary bosons but ultrabosons.

As the last remark in this section, this enhancement can be observed as an antibleaching effect on the photoinduced optical conductivity, in contrast to the ordinary bleaching effect. As is already mentioned, a strongly bound DH pair behaves like an ordinary boson, which leads to conventional bleaching effect in the photoinduced spectra. In contrast to this, a weakly bound pair and an unbound pair as an ultraboson are expected to show the enhancement for multiple excitations, which can be observed as an antibleaching effect, using femtosecond pump-probe experiments. Since the types of realized DH pairs depend on the degree of V, the variety of the photoinduced spectra will be observed after changing the materials systematically.

This paper is organized in the following way. The introduction is given in Sec. I. The model and the method are introduced in Sec. II. The third and fourth sections are dedicated to the results in the cases without and with the V term, respectively. The conclusions and discussions are given in the last section.

II. MODEL AND METHOD

To analyze the properties of DH pairs, we avoid the direct investigation of the extended Hubbard model and instead investigate the recently proposed charge model; both because the latter model enables calculations in a larger system and because of the substantial system-size dependency of the results, as will be shown later. The charge model is an effective model that extracts the charge degrees of freedom of the extended Hubbard model and successfully reproduces the optical conductivity spectra, down to at least $U/T \sim 5$ [30]. Here, T is the nearest-neighbor electron hopping.

The charge model is converted into a more convenient form as the previous definition only gives the matrix elements without a particle description. The procedure, explained in Appendix A, exactly converts the model into the following hard-core boson model:

$$
\begin{aligned}
H = &-T \sum_l (d_{l+1}^\dagger d_l + \text{h.c.}) - T \sum_l (h_{l+1}^\dagger h_l + \text{H.c.}) \\
&-\tilde{T} \sum_l \left((d_{l+1}^\dagger h_l^\dagger + h_{l+1}^\dagger d_l^\dagger) + \text{H.c.} \right) \\
&+(U/2) \sum_l \left(n_l^{(d)} + n_l^{(h)} \right) \\
&+V \sum_l n_l^{(d)} n_{l+1}^{(d)} + V \sum_l n_l^{(h)} n_{l+1}^{(h)}
\end{aligned}
$$

$$
\begin{aligned}
&-V \sum_l n_l^{(d)} n_{l+1}^{(h)} - V \sum_l n_l^{(h)} n_{l+1}^{(d)} \\
&+U_c \sum_l (d_l^\dagger d_l^\dagger d_l d_l + h_l^\dagger h_l^\dagger h_l h_l + d_l^\dagger d_l h_l^\dagger h_l), \quad (1)
\end{aligned}
$$

where d_l and h_l are the boson operators for a D and an H, respectively, with $n_l^{(d)} = d_l^\dagger d_l$ and $n_l^{(h)} = h_l^\dagger h_l$, $\tilde{T}$ is $\sqrt{2} C_s T$ with $C_s = 0.82$ [30], and U_c is taken as infinity.

We also mention the concrete definitions of the spectra treated here. First, the real part of the ordinary optical conductivity (one-photon optical conductivity) defined for the ground state ($|0\rangle$), namely, at zero temperature, is

$$
\sigma(\omega) = \frac{\gamma}{\pi \omega} \sum_{n>0} \frac{|\langle n|\hat{J}|0\rangle|^2}{(\omega - E_n + E_0)^2 + \gamma^2}, \quad (2)
$$

where E_n and $|n\rangle$ are the nth eigenenergy and the eigenstate, respectively, E_0 is the ground-state energy, and γ is the broadening factor. The definition of $\hat{J}$ is given in Appendix A. We neglect the Drude component because it is not relevant in this paper. Next we define two-photon optical conductivity, $\sigma^{(2)}(\omega)$, which is almost the same as $\sigma(\omega)$, although the ground state is replaced by the one-photon excited state, indexed as n_0, and the summation with respect to n has no restriction,

$$
\sigma^{(2)}(\omega) = \frac{\gamma}{\pi} \sum_n \frac{|\langle n|\hat{J}|n_0\rangle|^2}{\omega_{nn_0}} \frac{1}{(\omega - \omega_{nn_0})^2 + \gamma^2}, \quad (3)
$$

where ω_{nn_0} is E_n–E_{n_0}. In more detail, the one-photon excited state $|n_0\rangle$ is parity (P)-odd and charge-conjugation (CC)-odd in the charge model, while the allowed final state in $\sigma^{(2)}(\omega)$ is P-even and CC-even. This spectrum is different from the *true* optical conductivity, derived for the excited state using a linear response theory [38], which is

$$
\begin{aligned}
\sigma_{ex}(\omega) = \frac{\gamma}{\pi} \sum_n \frac{|\langle n|\hat{J}|n_0\rangle|^2}{\omega_{nn_0}} &\left\{ \frac{1}{(\omega - \omega_{nn_0})^2 + \gamma^2} \right. \\
&\left. + \frac{1}{(\omega + \omega_{nn_0})^2 + \gamma^2} \right\}.
\end{aligned} \quad (4)
$$

Note that the second term of Eq. (4), a de-excitation term, is negative for positive ω. For simplicity, we use the former expression predominantly in this paper. Regarding the numerical calculations, we follow a standard method; the ground state is determined by a Lanczos method [39] and the spectrum is calculated by a continued fraction [40].

III. CASES IN THE ABSENCE OF V

A. Overall features based on full calculations

Figure 1 shows the optical conductivity at excited states (red line), $\sigma^{(2)}(\omega)$, for $(U, V)/T = (10, 0)$ and a system size (N) of 16. This spectrum, defined in Eq. (3), is calculated by selecting the state corresponding to each peak of the ordinary optical conductivity (green lines), $\sigma(\omega)$, as the initial state (see the arrows). When the two spectra are compared for each case, the peaks of $\sigma^{(2)}(\omega)$ take the energies that almost correspond to those of $\sigma(\omega)$ in lower excitations, indicating that the two-DH-pair states are mostly a repetition of the initial
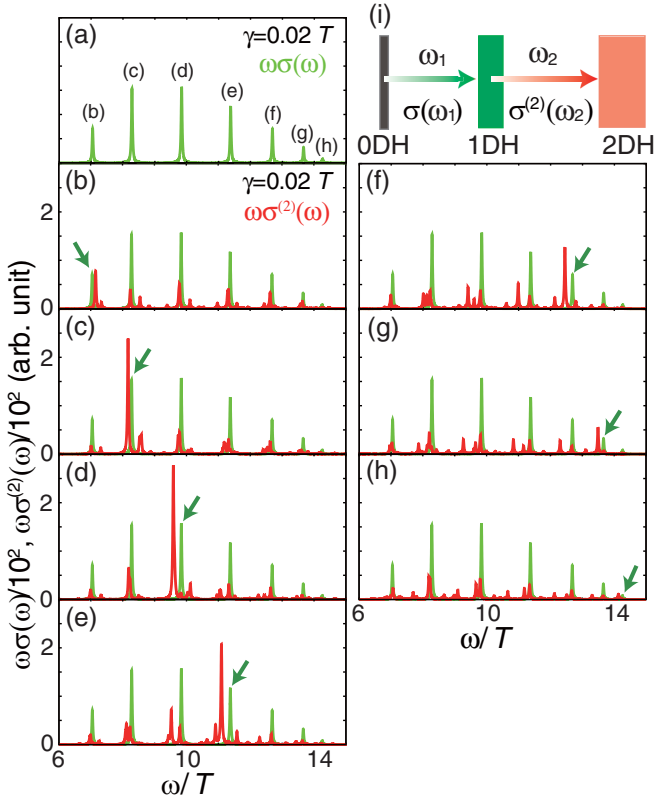
FIG. 1. (a) One-photon optical conductivity, $\sigma(\omega)$, calculated by the charge model with $(U, V)/T = (10, 0)$ and $N = 16$. The broadening factor γ is $0.02T$. (b)–(h) Two-photon optical conductivity (red curve), $\sigma^{(2)}(\omega)$, with $\sigma(\omega)$ (green curve). In each spectrum of $\sigma^{(2)}(\omega)$, the initial state is the state that corresponds to each peak of (a), as shown by the arrows. (i) Schematic for the two spectra.

pair. Furthermore, we see that an enhanced absorption peak appears at nearly the same energy as that of the initial excitation, except for the highest excitation, where the intensity of $\sigma(\omega)$ itself is very small. We find almost the same features also in the Hubbard model, as shown in Appendix B, and are confident that they are features common to both models.

B. Analyses based on approximate eigenfunctions

To interpret the above features, we propose approximate eigenfunctions for the excited states in the absence of V, which are considered useful to extract the physics behind the numerical results. First, the eigenfunctions for parity-odd one-DH-pair states are expressed as $|k\rangle = O^\dagger(k)|0\rangle$, with $O^\dagger(k) \equiv 1/\sqrt{2N}\sum_{li}(d_{l+i}^\dagger h_l^\dagger - h_{l+i}^\dagger d_l^\dagger)f_k(i)$ and $f_k(i) = (2/\sqrt{N})\sin(\pi ki/(N/2))$. Note that l takes the integers from 1 to N, while i and k from 1 to $(N-2)/2$. Regarding the parity-even two-DH-pair states, we express them using the same operator as $|k, k'\rangle = (1/\mathcal{N}_{k,k'})PO^\dagger(k)O^\dagger(k')|0\rangle$, where P is the projection that excludes more than one occupation of the particles at the same site and $\mathcal{N}_{k,k'}$ is the normalization factor that gives $\langle k, k'|k, k'\rangle = 1$. This assumption is based on the approximate nature found in the preceding subsection; the parity-even two-DH-pair states mostly as a repetition of the parity-odd one-DH-pair states. In principle, the former
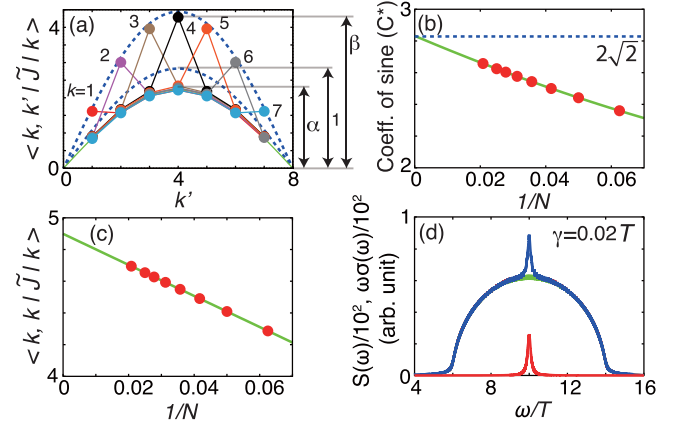

FIG. 2. (a) Matrix elements for $N = 16$. Upper and lower dashed curves follow $C\sin(\pi k'/(N/2))$, with $C = \pi\sqrt{2}$ and $2\sqrt{2}$, respectively. (b), (c) Fitting and extrapolations toward infinite N, with $k = N/4$. (d) Effective spectrum $S(\omega)$ (blue), $\omega\sigma(\omega)$ (green), and their difference (red).

states include the repetition of the parity-even one-pair states; however, such states are expected to arise from $|k, k'\rangle$, which is directly generated from $|k\rangle$, via electron-electron scattering. As can be determined from Fig. 1, this will not have a large effect.

Figure 2 shows the numerical results based on these approximate functions. In Fig. 2(a), the matrix element $\langle k, k'|\tilde{J}|k\rangle$ for $N = 16$ is plotted as a function of k' for various k's. The definition of the current operator $\tilde{J}$ is given in Appendix A. The enhancement at $k' = k$ for each curve over the background of $k' \neq k$ can be clearly seen. The one-photon matrix element, $\langle k'|\tilde{J}|0\rangle$, equal to $2\sqrt{2}\sin(\pi k'/(N/2))$, is plotted for comparison. The behaviors for other values of N, with $k = N/4$, are given in Appendix C. In Fig. 2(b), each background ($k' \neq k$) is fitted to $C^*\sin(\pi k'/(N/2))$ and its coefficient is plotted as a function of $1/N$. Figure 2(c) shows the enhancement plotted for $k = N/4$. In the limit of infinite N, the ratios, $\alpha \equiv C^*/(2\sqrt{2})$ and $\beta \equiv \langle k, k|\tilde{J}|k\rangle / \langle k|\tilde{J}|0\rangle$, are evaluated as 1.0013 and 1.7320, respectively. Although analytical estimation is difficult at this stage, these values suggest special numbers, namely, 1 and $\sqrt{3}$, respectively. In addition to the case $k = N/4$, we repeated these calculations for the case $k = N/8$ and the case in which the smallest k is selected for each N, to determine that both the cases also extrapolate to the same numbers, as described in Appendix C.

The following analysis attempts to understand the meanings of the above results, particularly, β. The expression for β is altered to

$$\beta = \langle k, k|\tilde{J}|k\rangle / \langle k|\tilde{J}|0\rangle$$
$$= \frac{1}{\mathcal{N}_{k,k}}\langle 0|O_k O_k P\sum_{k''}f_{k''}(1)O_{k''}^\dagger O_k^\dagger|0\rangle / f_k(1), \quad (5)$$

utilizing that $\tilde{J}$ can be expressed as $\sqrt{2N}\sum_k f_k(1)O_k^\dagger$. In this expression, the summation with respect to k'' is found to be limited to $k'' = k$ for infinite N, as shown in Appendix D, leading to the final expression $\beta = \mathcal{N}_{k,k}$. We also calculate

the normalization factor independently and find that

$$\lim_{N\to\infty}\mathcal{N}_{k,k'} = 1 \quad \text{for } k \neq k'$$
$$= \sqrt{3} \quad \text{for } k = k', \quad (6)$$

which is consistent with the estimation for β. A similar value for pure bosons, namely, $(1/\mathcal{N})\langle 0|BBB^\dagger B^\dagger|0\rangle$, where $\mathcal{N}$ is the norm of $B^\dagger B^\dagger|0\rangle$, is $\sqrt{2}$, indicating the unique property of the present operator. In our interpretation, this unique property originates from the variety in the formation of the two DH/HD pairs. For example, the sequential excitation of the DH and HD pairs leads most directly to DHHD, while they also lead to DHDH when DH contains HD, or to HDHD when vice versa. We emphasize that the particles in a pair can be apart to each other. Such states are superimposed on the directly formed DHDH(= DH + DH) or HDHD(= HD + HD), which is a coherent buildup of the coefficient.

Based on the above results, an effective spectrum for the two-pair part of $\omega\sigma_{\text{ex}}(\omega)$, $S(\omega)$, is defined as

$$S(\omega) = \frac{\gamma}{\pi}\left[\sum_{k_1\geqslant k_2}\frac{|\langle k_1,k_2|\tilde{J}|k_0\rangle|^2}{(\epsilon(k_1)+\epsilon(k_2)-\epsilon(k_0)-\omega)^2+\gamma^2} - \frac{|\langle k_0|\tilde{J}|0\rangle|^2}{(\epsilon(k_0)-\omega)^2+\gamma^2}\right], \quad (7)$$

with $\epsilon(k) = U - 4T\cos(\pi k/(N/2))$, shown in Fig. 2(d) for $N = 200$ and $k_0 = N/4$. As can be seen, $S(\omega)$ is enhanced at the band center despite the de-excitation term and the difference from $\omega\sigma(\omega)$ [41] is positive at the same position, taking the form of *antibleaching* [42].

C. Estimation of β using a minimum model and a full model

The discussion so far is based on the approximate eigenfunctions. We subsequently investigate the same property using a minimum model and a full model. The minimum model consists of subspaces of zero, one, and two DH pairs, with the couplings between them, $\tilde{T}$, set to zero. In principle, the corresponding part of the current operator is also zero; however, it is considered infinitesimally small and the ratio is taken as $\sum_{\mu_2\in S_c}|\langle\phi_{\mu_2}^{(2)}|\hat{J}|\phi_{\mu_1}^{(1)}\rangle/\langle\phi_{\mu_1}^{(1)}|\hat{J}|g\rangle|^2$, where $|\phi_{\mu_1}^{(1)}\rangle$ and $|\phi_{\mu_1}^{(2)}\rangle$ are the eigenfunctions of the one- and two-DH-pair states, respectively, and the S_c is the appropriate space of the degenerate final states. We first investigate the case of the initial excitation at the band center ($k = N/4$) in the absence of V. Here, the summation within the subspace S_c is calculated for the states with energy $2U$. This degeneracy does not disappear, even if the couplings between the subspaces are included. As shown in Fig. 3(a), the value equivalent to β^2 is extrapolated to 3, which is consistent with the result obtained by the approximate eigenfunctions. Regarding the excitation at $k = N/8$, we find separated peaks in addition to the main peaks, in $\sigma^{(2)}(\omega)$. Since there is no such degeneracy found for the band-center states, the accurate estimation of β is not easy due to the scattered intensities of the enhanced peak, which seem to be overlapped by those from the neighboring non-enhanced main peaks. In Appendix E, we show our preliminary estimation, based on the integrated intensities in an
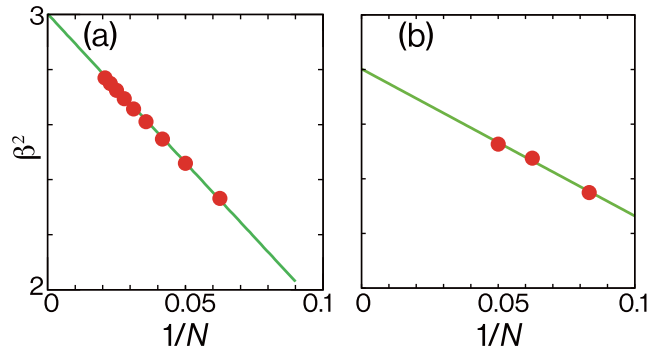

FIG. 3. Evaluation of β^2 values using (a) the minimum model and (b) the full model. The model parameters are $(U, V)/T = (10, 0)$ commonly.

interval, and find that the value of β^2 is substantially greater than 2.

The full model can be used to further check the results from the approximate eigenfunctions. The peak separation problem mentioned above is more serious in this case, and we find the same problem even at the excitation at the band center. Therefore, we try the same procedure for the minimum model with $k = N/8$; i.e., define an interval and take the ratio of the two integrated intensities of $\omega\sigma(\omega)$ and $\omega\sigma^{(2)}(\omega)$. Using the actual spectrum and the interval described in Appendix F, we obtain the N dependence of the intensity ratio, i.e., β^2, as shown in Fig. 3(b). The resulting extrapolated value is $\sim$2.8. Although the present largest size is limited as $N = 20$, the β^2 values much larger than two strongly suggest that antibleaching can be observed, despite the presence of actual fluctuation.

IV. CASES WITH FINITE V

In the following, we show the results found for finite V. First, we introduce arguments based on the approximate eigenfunctions. Here, we propose two types of states. The first type corresponds to the limiting case of strong DH binding, where the states are defined as $|\text{ex}\rangle \equiv O_{\text{ex}}^\dagger|0\rangle$ and $|2\text{ex}\rangle \equiv (1/\mathcal{N}_{\text{ex}})PO_{\text{ex}}^\dagger O_{\text{ex}}^\dagger|0\rangle$ for one- and two-DH-pair states with distance one, respectively, and $O_{\text{ex}}^\dagger \equiv (1/\sqrt{2N})\sum_l(d_{l+1}^\dagger h_l^\dagger - h_{l+1}^\dagger d_l^\dagger)$. The projection operator, P, is already defined, and $\mathcal{N}_{\text{ex}}$ is the norm of $|2\text{ex}\rangle$. In this case, we easily find that $\langle 2\text{ex}|\hat{J}|\text{ex}\rangle = \mathcal{N}_{\text{ex}}\langle\text{ex}|\tilde{J}|0\rangle$ and $\mathcal{N}_{\text{ex}} = \sqrt{2(N-3)/N}$. Note that the factor $(N-3)$ originates from the trivial fact that a neighboring DH excludes three sites for an additional neighboring pair. Note that we do not assume any interpair correlation, neglecting the formation of biexcitons. This simple result indicates that the above ratio (β for excitons) is $\sqrt{2}$ for infinite N, analogous to that of an ordinary boson. Another type of states are similar to those already used for $V = 0$; however, $f_k(i)$ is replaced with the eigenfunctions determined within the one-DH-pair space with $V = 3T$. Note that an excitonlike DH bound state is formed for this parameter as it exceeds the critical value of $V_c = 2T$. The resultant β^2 values are plotted (circles) with those of $2(N-3)/N$ (solid line) in Fig. 4(a). We clearly see that both the extrapolated values converge to 2 with high accuracy, indicating that a finite radius
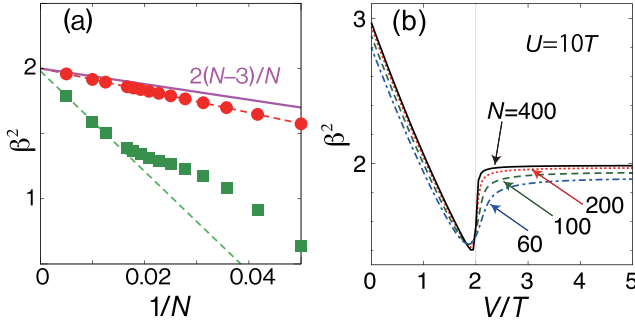
FIG. 4. (a) Evaluation of β^2 values using approximate functions and the minimum model for $(U, V)/T = (10, 3)$. The solid line is based on the simplest type of exciton function, while the exciton function is explicitly determined for circles. The squares show the results of the minimum model. (b) The evaluation of β^2, using approximate eigenfunctions for various V/T values. The system size is $N = 60, 100, 200,$ and 400, and U/T is fixed at 10.

of a DH bound state is irrelevant for this number, in the limit of infinite N.

To validate the above result, we also perform the evaluation using the minimum model. The minimum model is prepared in the same way as previously, except the V term takes $V = 3T$. Being common to the full fluctuation case, the enhanced part of the spectrum is not a single peak and requires a careful treatment. Most roughly speaking, the peaks separate into two peaks, which are assigned to DHDH- and DDHH-type states. In addition to these, we see scattered intensities originating from each peak. Therefore, we utilize a procedure that collects all the distributed intensities, as explained in Appendix G.

The resultant extrapolation from this procedure gives the same value as those by the approximate functions, although the behavior is not simple, as shown in Fig. 4(a) (squares). This complexity is thought to be related to the above two species (DHDH and DHHD). Specifically, when the size is smaller than a certain number around 60 ($1/N \sim 0.016$), the two states are nondegenerate and only one of the two peaks is considered in the estimation. When N is much larger than this number, the nondegeneracy disappears effectively within the resolution given by the present smallest γ, and combined peaks give an accurate extrapolation.

Thus far, our discussion has been limited to a strongly bound DH pair. Another interesting case is the opposite, in which the DH pair is either not formed or loosely bound in the presence of a weak V. To better understand this case, we again apply the approximate functions by changing V over a wide range. Figure 4(b) shows the behavior found for the cases with the first excitation fixed at the lowest energy. Common to all the system sizes, when we increase the V value, β^2 gradually decreases from three; the unusual value does not disappear suddenly, even if the effect of V is included. Such tendency continues as we approach $V_c = 2T$, i.e., the boundary of a bound DH pair and an unbound DH pair, where β^2 becomes less than two. Finally, for V larger than V_c, β^2 is fixed at approximately two, which is consistent with our previous result.

What is interesting is the β^2 values at V are slightly smaller than V_c. The N dependencies strongly suggest that this is a discontinuous transition at $V = V_c$. The two quantities giving
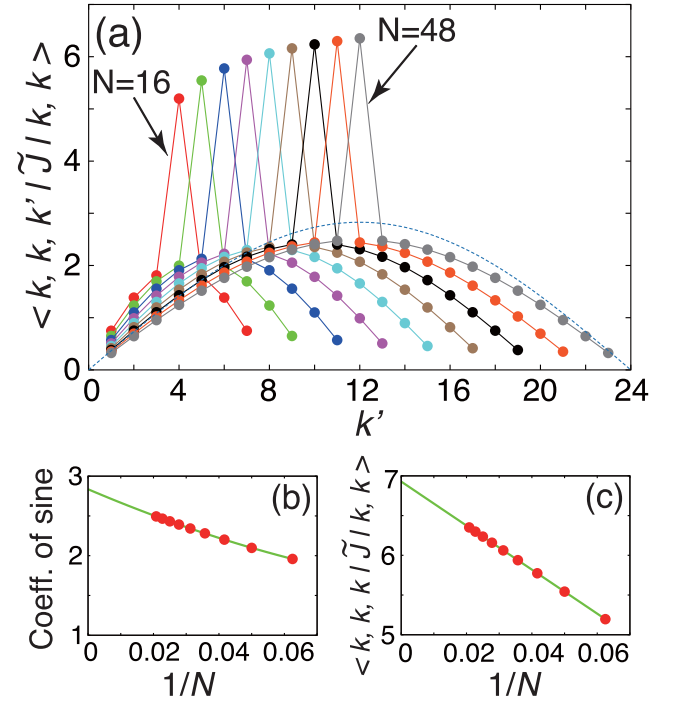

FIG. 5. Case of excitations from a two-DH-pair state to a three-DH-pair state. In (a), N is chosen as $N = 16, 20,..., 44,$ and 48, from left to right.

the ratio, β, are proportional to $\sqrt{N}$ for $V \leqslant V_c$, while they are of the order of one for $V > V_c$. We interpret that such an essential difference gives the discontinuity. Furthermore, when we closely check the form of the relevant function, $f_1(i)$, in the region of $V \leqslant V_c$, it gradually changes from that for $V = 0$ to that for $V = V_c$, which behave like $\sin(2\pi i/N)$ and $\cos(\pi i/N)$, respectively, for large N [43]. This is nothing but a change in the phase shift due to the increasing attraction between D and H. We speculate that this alters the degree of functional coherence as already mentioned, leading to different actual values of β. Meanwhile, the present assumption for the two-pair state neglects the repulsions between D and D (H and H). A more careful analysis beyond the approximate functions is required to give a quantitatively reliable result. In this respect, a preliminary analysis based on the minimum model reproduces a similar result. Namely, β values decrease monotonically in increasing V and finally becomes smaller than 2 near $V = V_c$, although completely converged results have not been obtained yet.

V. CASES OF FURTHER EXCITATIONS

Finally, the expected results of further excitations beyond two DH pairs are of further interest. Here, we restrict our analysis to three DH pairs; the states of $|k, k, k'\rangle \equiv (1/\mathcal{N}_{k,k,k'})PO_{k'}^\dagger O_k^\dagger O_k^\dagger |0\rangle$ in the form of approximate functions, with $k = N/4$. Figure 5(a) shows the associated matrix element, $\langle k, k, k'|\tilde{J}|k, k\rangle$, as a function of k', for $N = 16$–48. As expected, the enhancement occurs at the central position ($k' = N/4$), and the degree of enhancement is larger compared to the previous case. To

accurately determine the degree of enhancement, we again plot the behaviors in Figs. 5(b) and 3(c). The extrapolated values toward infinite N are $\alpha' = 1.00261$ and $\beta' = 2.44945$. Here, α' is defined similarly to α; as the ratio of the background amplitude to the one-photon amplitude, $2\sqrt{2}$. The value for α' is consistent with the previous value for α, which shows that the effect of existing excitations is zero in the limit of the infinite system size. The value for β', which is defined as $\beta' \equiv \langle k, k, k | \tilde{J} | k, k \rangle / \langle k | \tilde{J} | 0 \rangle$, is much larger than that for β. Interestingly, this number is very close to $\sqrt{6}$ ($=2.449489...$), suggesting that the latter is the true number. This number contrasts with the case of ordinary bosons having the corresponding number of $\sqrt{3}$, and the origin of this enhancement is again attributable to the variety of the DH patterns.

VI. CONCLUSIONS AND DISCUSSIONS

To conclude, we have found unique types of enhancements in the excitations of free or almost-free DH pair states. The factors are idealistically estimated as $\sqrt{3}$ and $\sqrt{6}$, for the excitations from one pair to two pairs and those from two pairs to three pairs, respectively. These numbers exceed the respective numbers for ordinary bosons, $\sqrt{2}$ and $\sqrt{3}$, from which we name the former ultrabosonic behaviors. These behaviors are suppressed to some degree in actual situations, while we find that the behaviors persist qualitatively in the presence of a typical amount of fluctuation. We think that the physical meaning of this behavior is worth deeper consideration. Below, we give an interpretation from a different viewpoint, mainly based on the results from the approximate eigenfunctions.

First, we discuss the case of two DH pairs. A simple hypothetical case assumes four independent bosons, in which one D(H) is converted to two D's (H's). In this case, the β^2 value is estimated at $(\sqrt{2})^2 = 4$ and we consider this number the maximum number. Meanwhile, the minimum number is given by the two excitons or the two strongly bound DH pairs, which is two as β^2. The effective number of particles is two in the latter case, being common to the ordinary boson picture of excitons in band insulators [44–47]. The present result for free or almost-free DH pairs as $\beta^2 = 3$ is the midpoint of these numbers, which suggests that the effective particle number is intermediate. The same remark is also made on the three DH pairs; the maximum (minimum) number is nine (three), while the present result gives six, again being the midpoint. All these results seem to indicate that the ultrabosonic behavior is deeply related to the effective particle number elevated from that for the exciton case up to the half that of the hypothetical case.

In relation to experiments, we expect that the ultrabosonic behaviors can be observed as a signature of antibleaching in the photoinduced spectra. As already mentioned, the V value should be small for this purpose, and the selection of the materials will be critical.

On the basis of the above findings, we now have a special interest in the possibility of realizing a condensate of free or almost-free DH pair states. The enhanced factors for multiple DH pairs have a possibility to drive such a condensate, particularly at low-energy excitations. Such *ultrabosonic* nature of DH pairs is expected to further new possibilities in the
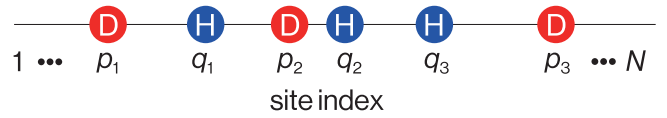

FIG. 6. Example of the number used in Eq. (A1). In this example, ($M = 3$), τ is $0 + 1 + 3 = 4$.

study of the nonequilibrium properties of strongly correlated electron systems.

APPENDIX A: MODEL TRANSFORMATION FROM THE ORIGINAL MODEL TO THE HARD-CORE BOSON MODEL

A merit of the charge model introduced in Ref. [30] is its extraction of the charge degrees of freedom; however, it has a complicated definition of the Hamiltonian matrix elements. To make the model useful by expressing it in a particle picture, we transform it in the following way. First, we define the factor as

$$S \equiv (-1)^{\sum_{i=1}^{M} p_i}(-1)^{\tau} \tag{A1}$$

for each basis state in the charge model, and define a new basis state as

$$
\begin{aligned}
&|\{p_1, p_2, ..., p_M\}, \{q_1, q_2, ..., q_M\}\rangle_{\text{new}} \\
&\equiv S\,|\{p_1, p_2, ..., p_M\}, \{q_1, q_2, ..., q_M\}\rangle, \tag{A2}
\end{aligned}
$$

where τ is the summation of the number of H's on the left of each D, and $\{p_i\}$ and $\{q_i\}$ are the positions of D and H, respectively (an example is illustrated in Fig. 6). Using this transformation, we cancel complicated signs in the original model, resulting in an equivalent model appearing in Eq. (1) of the main text.

We also introduce the definition of the current operator in the hard-core boson model as

$$
\begin{aligned}
\hat{J} = iT\sum_{l=1}^{N}(d_{l+1}^{\dagger}d_l - \text{h.c.}) - iT\sum_{l=1}^{N}(h_{l+1}^{\dagger}h_l - \text{H.c.}) \\
+ i\tilde{T}\sum_{l=1}^{N}((d_{l+1}^{\dagger}h_l^{\dagger} - h_{l+1}^{\dagger}d_l^{\dagger}) - \text{H.c.}), \tag{A3}
\end{aligned}
$$

which is automatically derived from the current operator defined in the charge model. Another form of the current operator ($\tilde{J}$) contains only the part associated with the creation of a DH-pair, namely,

$$\tilde{J} = i\tilde{T}\sum_{l=1}^{N}(d_{l+1}^{\dagger}h_l^{\dagger} - h_{l+1}^{\dagger}d_l^{\dagger}). \tag{A4}$$
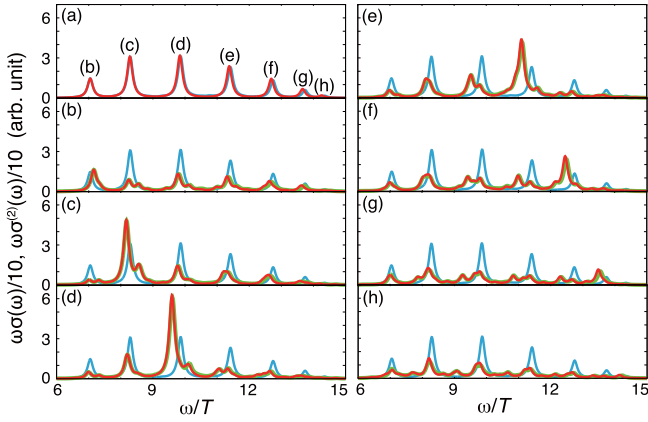
FIG. 7. $N = 16$, $U = 10T$, $V = 0$, $\gamma = 0.1T$. Blue lines in (a)–(h) are $\omega\sigma(\omega)$ of the half-filled Hubbard model. Green lines in (b)–(h) are $\omega\sigma^{(2)}(\omega)$ of the half-filled Hubbard model. Red lines are $\omega\sigma(\omega)$ in (a) and $\omega\sigma^{(2)}(\omega)$ in (b)–(h) of the charge model ($M_{\max} = 8$). Initial states of calculating $\omega\sigma^{(2)}(\omega)$ in (b)–(h) are corresponding excited states at the peaks of $\omega\sigma(\omega)$ in (a).

We use this definition for the matrix elements associated with the approximate eigenstates.

APPENDIX B: COMPARISON OF THE OPTICAL SPECTRA OF THE HUBBARD MODEL AND THE CHARGE MODEL

In our previous work [30], we found that the charge model reproduces the one-photon optical conductivity satisfactorily. In this paper, we have also checked the feasibility of the charge model from the viewpoint of $\sigma^{(2)}(\omega)$ via the comparison with that of the Hubbard model. In Figs. 7(b)–7(h), we summarize the results for $\sigma^{(2)}(\omega)$ for $N = 16$, in which each peak of $\sigma(\omega)$ in Fig. 7(a) is assumed as the initial state. For $\sigma(\omega)$, we again confirm that both the results, i.e., those from the Hubbard model and the charge model, coincide with each other satisfactorily. Regarding $\sigma^{(2)}(\omega)$, we also find good coincidences in Figs. 7(b)–7(h). Based on these results, we can say that the charge model accurately describes the excited states up to at least two-photon excitations.

APPENDIX C: DETAILS OF THE RESULTS USING THE APPROXIMATE EIGENSTATES

Here we describe the results that are based on the approximate eigenstates but are not explained in detail in the main text. Figure 8 shows the specific behaviors of the matrix element for the excitation at $k = N/4$. The extrapolations in Figs. 2(b) and 2(c) of the main text are made based on this plot. We then discuss the cases in which the initial state is set at other k modes. As shown in Fig. 2(a), the concerned enhancement occurs at every k mode, for a value of N of at least 16. Here, we focus on the following two cases and discuss the details of their behaviors, including N dependency. The first case is $k = N/8$. Figure 9(a) shows $\langle k, k'|\tilde{J}|k\rangle$ for $N = 16$–48, and the same quantities used for the case of $k = N/4$ are evaluated and plotted in Figs. 9(b) and 9(c). According to these figures, the α and β values for infinite N are 0.999658 and 1.731617; close to 1 and $\sqrt{3}$, respectively. In
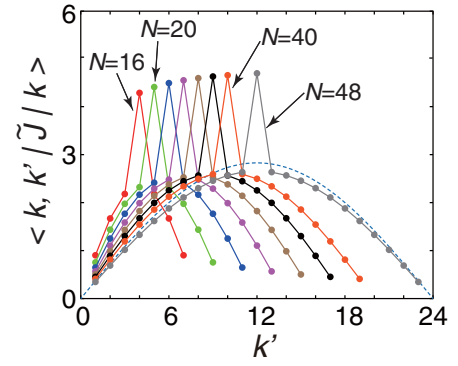
the second case, the excitation is set at the $k = 1$ mode. Note that the wave number, $\pi/(N/2)$, changes depending on N, in contrast to the other two cases of $k = N/4$ and $N/8$, where the wave numbers are fixed at $\pi/2$ and $\pi/4$, respectively. In spite of this complexity, the extrapolations successfully give the results of $\alpha = 1.00206$ and $\beta = 1.7345$, as shown in Figs. 9(d) and 9(e), which are again close to 1 and $\sqrt{3}$, respectively.
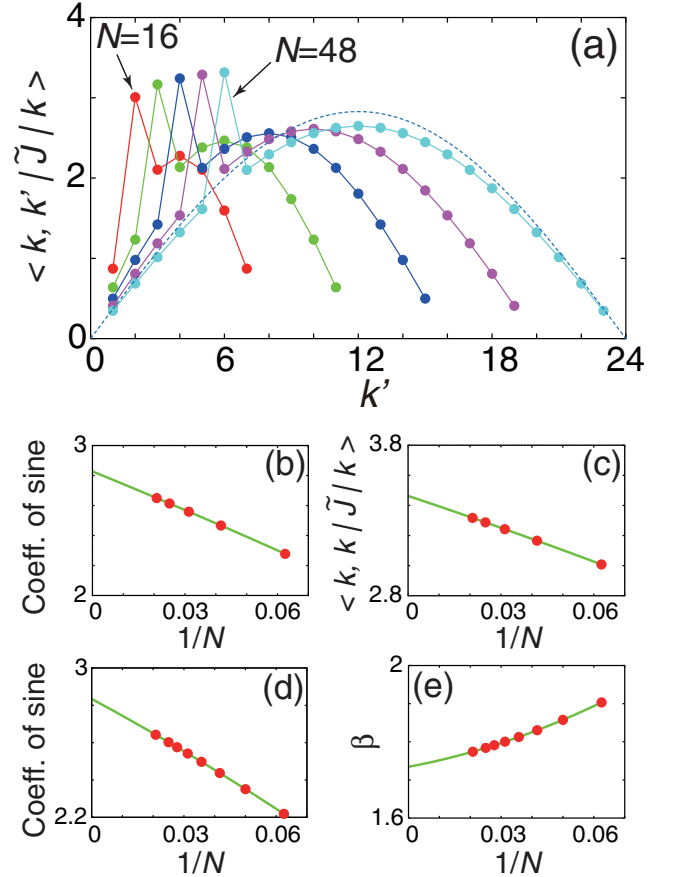

FIG. 8. Details of the extrapolation $k = N/4$. The lines are for $N = 16, 20, 24,..., 40$, and 48, from left to right.

FIG. 9. Details of the extrapolation for (a)–(c) $k = N/8$ with $N = 16, 24, 32, 40$, and 48, and (d) and (e) for the lowest k at each N ($k = 1$).
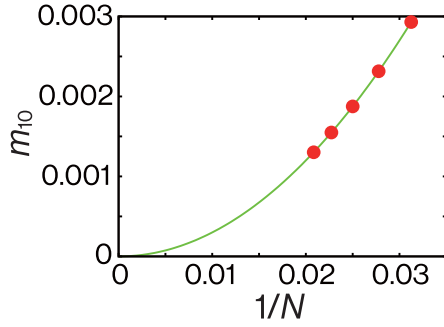
FIG. 10. Extrapolation of the absolute value of the non-zero off-diagonal matrix element, m_{10}.

APPENDIX D: MATRIX ELEMENT OF THE FOUR-OPERATOR PRODUCT

We discuss the following matrix element:

$$M_{k',k} \equiv \langle 0| O_k O_k P O_{k'}^\dagger O_k^\dagger |0\rangle \ , \qquad (D1)$$

where $O_k^\dagger$ is the creation operator of an odd-parity DH pair defined as

$$O^\dagger(k) \equiv \frac{1}{\sqrt{2N}} \sum_{li} (d_{l+i}^\dagger h_l^\dagger - h_{l+i}^\dagger d_l^\dagger) f_k(i) \ , \qquad (D2)$$

where $f_k(i) = (2/\sqrt{N}) \sin(\pi k i/(N/2))$, and k and k' take integers between 1 and $N_{\text{mode}} (= (N-2)/2)$. We calculate this matrix element for each N and find that the element remains finite, with the exception of the diagonal element and one special off-diagonal element. Other elements are of the orders of 10^{-15} or less in the double precision are considered to be zero. In more detail, the matrix elements, with the exception of the negligible ones, are written for $N = 4n$ (n is an integer) as

$$M_{k',k} = m_0 \delta_{k',k} + m_1(k)\delta_{k',k^*(k)} \ , \qquad (D3)$$

where m_0 is a constant, and $k^*(k)$ is the row number as a function of k. Furthermore, using the definition of the *inverted* number for k, i.e., $k_I = N_{\text{mode}} + 1 - k$, k^* and m_1 are determined by the following conditions:
(1) If $3k \leqslant N_{\text{mode}}$, $k^* = 3k$ and $m_1(k) = -m_{10}$.
(2) If $N_{\text{mode}} + 1 - 3k_I \geqslant 1$, $k^* = N_{\text{mode}} + 1 - 3k_I$ and $m_1(k) = -m_{10}$.
(3) If $k = n \pm 3l$ and $1 \leqslant n \pm 3l \leqslant N_{\text{mode}}$, $k^* = n \mp 3l$ and $m_1(k) = m_{10}$.
Here, m_{10} is a finite positive constant, and l is a positive integer. We emphasize that the above conditions are exclusive to one another and select only one k^* for each k in most cases. (One exception is the case for $N_{\text{mode}} = 3r + 2$ (r is an integer), where no k^* is selected for two particular columns.) In Fig. 10, we plot m_{10} as a function of $1/N$. The curve is very accurately fitted with a parabolic function, indicating that the extrapolated value for infinite N is zero; this shows that $M_{k',k}$ is a diagonal matrix in the same limit.
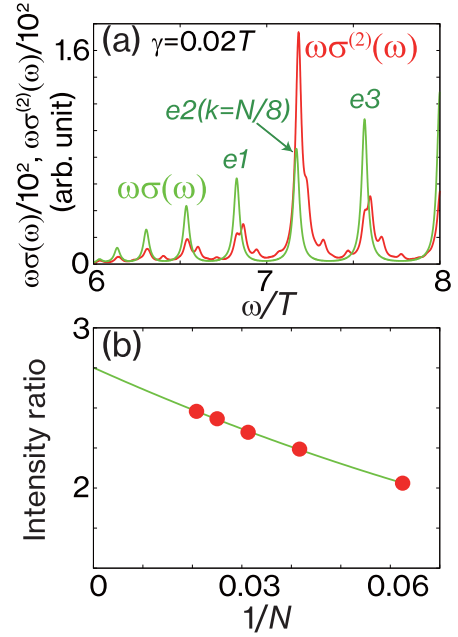

FIG. 11. Details of the analysis using the minimum model for excitation at $k = N/8$. (a) Spectra for $N = 48$ with $(U, V)/T = (10, 0)$ and $\gamma = 0.02T$. The three peak energies of $\omega\sigma(\omega)$, $e1 \sim e3$, are defined in the main text. (b) Extrapolation of the intensity ratio toward infinite N.

APPENDIX E: DETAILS OF THE EXTRAPOLATION USING THE MINIMUM MODEL: CASE OF $V = 0$ AND THE $k = N/8$ EXCITATION

We investigate the case of $k = N/8$ for $V = 0$. First, we define three peak energies of $\omega\sigma(\omega)$, as shown in Fig. 11(a). The peak energy of $\omega\sigma(\omega)$ with $k = N/8$ is denoted as $e2$, while the neighboring peaks with $k = N/8-1$ and $k = N/8 + 1$ as $e1$ and $e3$, respectively. We integrate $\omega\sigma(\omega)$ and $\omega\sigma^{(2)}(\omega)$ in the interval of $[(e1 + e2)/2, (e2 + e3)/2]$ and plot the ratio as a function of $1/N$, as shown in Fig. 11(b). Via extrapolation, the value for infinite N is evaluated as 2.7515, which is thought to give a rough estimate of β^2.
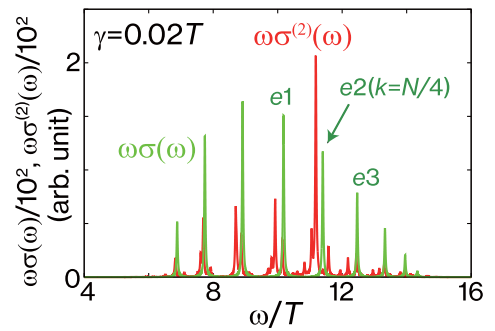

FIG. 12. Spectra of the full model with $(U, V)/T = (10, 0)$. The other parameters are $N = 20$ and $\gamma = 0.02T$. $e1 \sim e3$ are defined in the main text. The integrated intensities in $[(e1 + e2)/2, (e2 + e3)/2]$ are used to obtain Fig. 3(b) in the main text.
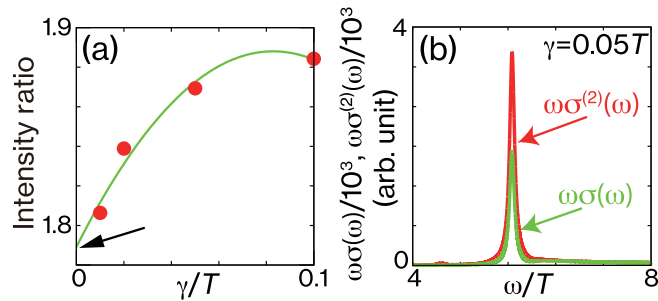
FIG. 13. Details of the extrapolation using the minimum model with $(U, V)/T = (10, 3)$. (a) Dependence of the intensity ratio on the γ value. (b) Spectra for $N = 200$.

APPENDIX F: DETAILS OF THE EXTRAPOLATION USING THE FULL MODEL: CASE OF $V = 0$ AND THE $k = N/4$ EXCITATION

We show the spectra for $N = 20$ in Fig. 12, as examples. These are obtained using $(U, V)/T = (10, 0)$ and $\gamma = 0.02T$. The interval in which the intensities are integrated is $[(e1 + e2)/2, (e2 + e3)/2]$, where the peak energy of $\omega\sigma(\omega)$ with $k = N/4$ is denoted as $e2$, while the neighboring peaks

with $k = N/4 - 1$ and $k = N/4 + 1$ as $e1$ and $e3$, respectively. The resultant intensities and the ratio between them are used for the plot in Fig. 3(b).

APPENDIX G: DETAILS OF THE EXTRAPOLATION USING THE MINIMUM MODEL: CASE OF FINITE V

We discuss the case for finite V, using the minimum model. In contrast to the preceding case, $V = 0$, there is no well-defined interval in which the spectral intensities should be integrated. Therefore, we resort to another method, explained in the following. As already mentioned in the main text, the peak is not a pure single peak but instead consists of many peaks. First, we must exclude the effects of the peaks that are not relevant in the present estimation. To do so, we vary γ in a finite interval and determine the extrapolated value toward $\gamma = 0$. Figure 13(a) shows such γ dependence for $(U, V)/T = (10, 3)$ with $N = 200$. The example spectra for $\gamma = 0.05T$ are shown in Fig. 13(b). Here, the largest size is increased to $N = 200$ as the previous largest size, $N = 48$, is insufficient due to a more complicated N-dependency, as shown in Fig. 4(a).

[1] K. Nasu, *Photoinduced Phase Transitions* (World Scientific, Singapore, 2004).

[2] *The One-Dimensional Hubbard Model*, F. H. L. Essler, H. Frahm, F. Göhmann, A. Klümper, and V. Korepin (Cambridge University Press, Cambridge, 2010).

[3] M. Ogata and H. Shiba, Phys. Rev. B **41**, 2326 (1990).

[4] S. Tomonaga, Prog. Theor. Phys. **5**, 544 (1950).

[5] J. M. Luttinger, J. Math. Phys. **4**, 1154 (1963).

[6] D. C. Mattis and E. H. Lieb, J. Math. Phys. **6**, 304 (1965).

[7] J. Sólyom, Adv. Phys. **28**, 201 (1979).

[8] F. D. M. Haldane, J. Phys. C: Solid State Phys. **14**, 2585 (1981).

[9] H. J. Schulz, Int. J. Mod. Phys. B **5**, 57 (1991).

[10] J. Voit, Rep. Prog. Phys. **58**, 977 (1994).

[11] W. Stephan and K. Penc, Phys. Rev. B **54**, R17269 (1996).

[12] E. Jeckelmann, F. Gebhard, F. H. L. Essler, Phys. Rev. Lett. **85**, 3910 (2000).

[13] H. Kishida, H. Matsuzaki, H. Okamoto, T. Manabe, M. Yamashita, Y. Taguchi, and Y. Tokura, Nature (London) **405**, 929 (2000).

[14] T. Ogasawara, M. Ashida, N. Motoyama, H. Eisaki, S. Uchida, Y. Tokura, H. Ghosh, A. Shukla, S. Mazumdar, and M. Kuwata-Gonokami, Phys. Rev. Lett. **85**, 2204 (2000).

[15] Y. Mizuno, K. Tsutsui, T. Tohyama, and S. Maekawa, Phys. Rev. B **62**, R4769 (2000).

[16] H. Kishida, M. Ono, K. Miura, H. Okamoto, M. Izumi, T. Manako, M. Kawasaki, Y. Taguchi, Y. Tokura, T. Tohyama, K. Tsutsui, and S. Maekawa, Phys. Rev. Lett. **87**, 177401 (2001).

[17] M. Ono, K. Miura, A. Maeda, H. Matsuzaki, H. Kishida, Y. Taguchi, Y. Tokura, M. Yamashita, and H. Okamoto, Phys. Rev. B **70**, 085101 (2004).

[18] H. Matsueda, N. Bulut, T. Tohyama, and S. Maekawa, Phys. Rev. B **72**, 075136 (2005).

[19] K. Iwano, Phys. Rev. Lett. **97**, 226404 (2006).

[20] S. Wall, D. Brida, S. R. Clark, H. P. Ehrke, D. Jaksch, A. Ardavan, S. Bonora, H. Uemura, Y. Takahashi, T. Hasegawa, H. Okamoto, G. Cerullo, and A. Cavalleri, Nat. Phys. **7**, 114 (2011).

[21] M. Eckstein and P. Werner, Phys. Rev. B **84**, 035122 (2011).

[22] H. Matsueda, S. Sota, T. Tohyama, and S. Maekawa, J. Phys. Soc. Jpn. **81**, 013701 (2012).

[23] Z. Lenarčič and P. Prelovšek, Phys. Rev. Lett. **111**, 016401 (2013).

[24] M. Eckstein and P. Werner, Phys. Rev. Lett. **110**, 126401 (2013).

[25] E. Iyoda and S. Ishihara, Phys. Rev. B **89**, 125126 (2014).

[26] M. Mitrano, G. Cotugno, S. R. Clark, R. Singla, S. Kaiser, J. Stähler, R. Beyer, M. Dressel, L. Baldassarre, D. Nicoletti, A. Perucchi, T. Hasegawa, H. Okamoto, D. Jaksch, and A. Cavalleri, Phys. Rev. Lett. **112**, 117801 (2014).

[27] D. Golež, J. Bonča, M. Mierzejewski, and L. Vidmar, Phys. Rev. B **89**, 165118 (2014).

[28] Z. Lenarčič and P. Prelovšek, Phys. Rev. B **90**, 235136 (2014).

[29] R. Singla, G. Cotugno, S. Kaiser, M. Först, M. Mitrano, H. Y. Liu, A. Cartella, C. Manzoni, H. Okamoto, T. Hasegawa, S. R. Clark, D. Jaksch, and A. Cavalleri, Phys. Rev. Lett. **115**, 187401 (2015).

[30] S. Ohmura, A. Takahashi, K. Iwano, T. Yamaguchi, K. Shinjo, T. Tohyama, S. Sota, and H. Okamoto, Phys. Rev. B **100**, 235134 (2019).

[31] T. Miyamoto, T. Kakizaki, T. Terashige, D. Hata, H. Yamakawa, T. Morimoto, N. Takamura, H. Yada, Y. Takahashi, T. Hasegawa, H. Matsuzaki, T. Tohyama, and H. Okamoto, Commun. Phys. **2**, 131 (2019).

[32] S. Iwai, M. Ono, A. Maeda, H. Matsuzaki, H. Kishida, H. Okamoto, and Y. Tokura, Phys. Rev. Lett. **91**, 057401 (2003).

[33] H. Okamoto, H. Matsuzaki, T. Wakabayashi, Y. Takahashi, and T. Hasegawa, Phys. Rev. Lett. **98**, 037401 (2007).

[34] A. Takahashi, H. Itoh, and M. Aihara, Phys. Rev. B **77**, 205105 (2008).

[35] T. Kaneko, T. Shirakawa, S. Sorella, and S. Yunoki, Phys. Rev. Lett. **122**, 077002 (2019).

[36] J. M. Leinaas and J. Myrheim, Il Nuovo Cimento B **37**, 1 (1977).

[37] F. Wilczek, Phys. Rev. Lett. **49**, 957 (1982).

[38] N. Maeshima and K. Yonemistu, J. Phys. Soc. Jpn. **74**, 2671 (2005).

[39] Y. Saad, *Iterative Methods for Sparse Linear Systems*, 2nd ed. (Society for Industrial and Applied Mathematics, Philadelphia, 2003).

[40] E. R. Gagliano and C. A. Balseiro, Phys. Rev. Lett. **59**, 2999 (1987).

[41] $\omega\sigma(\omega)$ is defined here as $(\gamma/\pi)\sum_k |\langle k|\tilde{J}|0\rangle|^2/((\omega-\epsilon(k))^2 + \gamma^2)$.

[42] The positive difference in this part does not violate the so-called sum rule because there are other parts such as those related to one-pair to one-pair transitions.

[43] The exact functional form at $V = V_c$ is $(2/\sqrt{N-1})\cos[\pi(i-1/2)/(N-1)]$.

[44] I. Carusotto and C. Ciuti, Rev. Mod. Phys. **85**, 299 (2013)

[45] T. Byrnes, N. Y. Kim, and Y. Yamamoto, Nat. Phys. **10**, 803 (2014).

[46] M. A. Bastarrachea-Magnani, A. Camacho-Guardian, M. Wouters, and G. M. Bruun, Phys. Rev. B **100**, 195301 (2019).

[47] Y. Murakami, M. Schüler, S. Takayoshi, and P. Werner, Phys. Rev. B **101**, 035203 (2020).